Smart metacomposite-based systems for transient elastic wave energy harvesting

Kaijun Yi, Mélodie Monteil, Manuel Collet, Simon Chesné

Smart metacomposite-based systems for transient elastic wave energy harvesting

K. Yi[a], M. Monteil[b], M. Collet[a,*], S. Chesne[b]

[a] *LTDS UMR5513 Ecole Centrale de Lyon, 36 Avenue Guy de Collongue, 69130 Ecully, France*
[b] *Université de Lyon, CNRS INSA-Lyon, LaMCoS UMR5259, F-69621 Villeurbanne, France*

Abstract

In this paper, novel harvesting systems are proposed and studied to obtain enhanced energy from transient waves. Each of these systems contains a piezo-lens to focus waves and a harvester to yield energy from the induced focused waves. The piezo-lens comprises a host plate and piezoelectric patches bonded on the plate surfaces. The piezoelectric patches are shunted with negative capacitance (NC) circuits in order to control the spatial variation of the effective refractive index inside the piezo-lens domain. The harvester is placed at the designed focal point of the piezo-lens, two different SSHI (synchronized switch harvesting on inductor) based harvesters are analyzed in the studies. Corrected reduced models are developed to predict the transient responses of the harvesting systems. The performances of the systems incorporating SSHI-based harvesters in transient wave energy harvesting are studied and compared with the system using a standard DC harvester. The focusing effect of the piezo-lens on transient waves and its capability to improve the harvested energy are verified. Since the NC circuits are active elements, an energy balance analysis is performed. Applicability of the harvesting systems is also discussed.

Keywords: piezoelectric material, negative capacitance, model reduction, wave focusing, energy harvesting, SSHI (synchronized switch harvesting on inductor) interface

1. Introduction

Design more reliable, durable and comfortable products is a long-term objective in modern industries, such as aerospace, transport and civil engineering. Nowadays, with the rapid development in electronics, computer science and material science, smart structures are proposed in an attempt to achieve this goal [1]. Smart structures are hybrid systems composed of load-bearing materials and electronic units like but not limited to control and health monitoring units. An electronic unit typically contains sensors, actuators, computing devices and communication module, all these devices require power supply. Traditional batteries are not suitable choices due to their limited life spans, which will lead to maintenance problems. A more appropriate way is to integrate energy harvesting devices into the smart structures to realize self-powered systems.

Due to the ubiquitous presence of vibration in structures, extensive efforts have been made to harvest vibration energy [2]. Among these studies, a lot of them were dedicated

*Corresponding author
Email address: manuel.collet@ec-lyon.fr (M. Collet)

to obtain higher harvesting efficiency and/or to extend the operating frequency band of the harvesting system. Examples include (i) tuning the harvesting system through passive or active methods to match the operating frequency with the environment [3, 4]; (ii) exploiting nonlinear mechanical mechanisms to widen the operating frequency band [5]; (iii) using phononic crystals [6], metamaterials [7] or acoustic black holes [8] to increase energy densities near the harvesters.

Apart from the mechanical approaches, nonlinear energy extraction circuits have been proposed to boost the harvested energy when piezoelectric transducers are used. The introduced nonlinear part is termed "synchronized switch harvesting on inductor" (SSHI) interface, which is composed of a switch and an inductor in series. The switch is turned off when the voltage of the piezoelectric transducer reaches a minimum or a maximum. Under this situation, the inductance and the capacitance constitute an oscillating circuit with a period much smaller than the mechanical one. After a very short time equals to a half of the period of the oscillating circuit, the switch is turned on again. Consequently, the voltage is inverted. The SSHI interface only requires a small amount of power to control the switch, it could be self-powered [9].

The SSHI interface is firstly proposed and studied by D. Guyomar et al.[10], and has drawn considerable attention these years. It is connected with the piezoelectric element in parallel to form a parallel SSHI harvesting system [10–13], or in series to obtain a series SSHI harvesting system [11, 12]. Researches show that the SSHI interface can improve the converted energy by the piezoelectric transducer from mechanical to electrical form and reduce the backward conversion [14]. In a weekly coupled electromechanical system, the harvested power is boosted by 4 to 9 times when compared to a standard DC technique proposed by G. Ottman et al [15]. In a strongly coupled case, these techniques will produce almost equivalent power but the required piezoelectric materials for the SSHI-based techniques are much less [10]. Based on the SSHI interface, several improved techniques have been proposed, each of them addresses a particular concern. Such as the "double synchronized switch harvesting" (DSSH) [16] and the "enhanced synchronized switch harvesting" (ESSH) [17] are proposed to obtain load independent techniques. The "adaptive synchronized switch harvesting" (ASSH) [18] technique is developed to harvest energy in multimodal vibration situations. The characteristics, advantages and drawbacks of these SSHI-based techniques are discussed in details by D. Guyomar et al. [9].

Harvesting vibration energy in structures is well studied, however limited effort has been devoted to harvest energy from traveling waves. Traveling waves are common in built-up structures, since the power in these structures transmits from one component to another especially at higher frequency bands [19, 20]. In addition, waves will propagate away from the source when structures are under non stationary excitations, they are attenuated by damping and/or radiation thus are not reflected back to the source to form standing waves. It is important to develop harvesting systems to obtain energy from waves in those cases.

To harvest energy from traveling waves, one of the main challenges is that the amount of harvested energy could be very low. In recent years, to increase harvested energy from traveling waves, several innovative harvesting systems have been developed [21–24]. The fundamental idea is to steer waves to increase the energy densities at particular positions and harvest there. For examples, an elliptical acoustic mirror or a parabolic acoustic mirror is used to focus waves in the systems proposed by [21–23]; in [23], an artificial periodic array with a defect is designed to localize energy at specific frequencies, an acoustic funnel formed by arrays of acoustic scatters is developed to guide waves into a narrow channel. However,

the harvesting circuits in these studies are simply represented by resistive ones in order to focus analysis in the mechanical part of the system. This is acceptable from an academic point of view but not adequate in practice since most of the real-life low power electronic devices require DC, the actual harvesting circuit always contains a AC-to-DC converter and maybe some other nonlinear parts, which can't be simplified as a linear resistive load.

Different from the aforementioned methods to steer waves, recently a piezo-lens is proposed to focus waves [25]. The piezo-lens is composed of a host plate and several surface-bonded piezoelectric patches. These patches are shunted with negative capacitance (NC) circuits. The spatial variation of refractive index in the piezo-lens zone is designed to fulfill a hyperbolic secant profile. Results show that the piezo-lens can focus flexural waves near a designed point in a broad frequency band. Thus the piezo-lens has large potential to be exploited in developing advanced harvesting systems for waves.

In this paper, the piezo-lens is combined with SSHI-based harvesters to improve the harvested energy from transient waves. An analytical relationship which connects the effective refractive index of piezoelectric system to the shunting NC value is used to design the piezo-lens; corrected reduced models are developed to predict the transient responses of the piezoelectric systems. With these tools, the performances of the harvesting systems are studied and discussed.

2. Configuration of the harvesting system

2.1. The first part: a piezo-lens

The harvesting system proposed in this paper consists in the combination of a piezo-lens and a harvester. The concept and designing process of the piezo-lens are introduced in this section. The piezo-lens is obtained by periodically bonding piezoelectric patches on the surfaces of a host aluminum plate in a collocated fashion, as depicted in figure 1(a). The host plate is lying in the $x-y$ plane and occupying the spatial region $-h_b/2 \leq z \leq h_b/2$. The piezo-lens zone could be divided into a 14-by-6 array of piezoelectric cell, the patches in each of these cells are shunted with a NC circuit and their bonding surfaces are grounded, as shown in figure 2.

To focus flexural waves, the spatial variation of the refractive index of flexural wave inside the piezo-lens zone is designed to fulfill a hyperbolic secant function:

$$n(y) = n_0 \cdot sech(\alpha(y-\beta)) \tag{1}$$

in which, n_0 represents the refractive index of the background plate, α is the gradient coefficient and β represents the y coordinate of the symmetry axis of the refractive index profile, as illustrated in figure 1(b). Due to this design, waves incident into the lens from the Ox direction will be focused at a focal point at the $y = \beta$ line, with a focal length $f = \pi/2\alpha$ measuring from the left boundary of the lens [26].

By tuning the NC values, one can change the local dynamic properties where piezoelectric patches are bonded [7, 25]. Thus, the variation of the refractive index inside the piezo-lens can be approximately realized in a piecewise form by designing the NC values of cells at different locations. According to equation (1), the refractive index only varies in the y direction. Thus, in a piezo-lens, the shunting NC values are equal in a same row (the x direction) but will differ in a same column (the y direction). To determine the required shunting NC value in each row, an analytical relationship between the effective refractive index of the cell and the NC value is developed.

The relationship is obtained in four steps. In the first step, the effective Young's modulus and effective Poisson's ratio of the piezoelectric patches shunted with NC are represented as functions of the NC value:

$$\begin{aligned} E_p &= E_p^{sh}\frac{C_{neg}+C_p^T}{C_{neg}+C_p^T(1-k_{31}^2)} \\ \mu_p &= \mu_p^{sh}\frac{C_{neg}+C_p^T(1+k_{31}^2/\mu_p^{sh})}{C_{neg}+C_p^T(1-k_{31}^2)} \end{aligned} \tag{2}$$

here, E_p^{sh} and μ_p^{sh} stand for the Young's modulus and the Poisson's ratio of the short-circuit piezoelectric material, respectively; k_{31} is the coupling factor; C_p^T is the free intrinsic capacitance (namely the capacitance when the patch is under constant stress); C_{neg} is the applied NC value.

In the second step, the effective parameters of the shunted piezoelectric sandwich structure highlighted by the dashed lines in figure 2 are determined according to the classical laminated plate theory [27]. The effective area density and effective flexural rigidity of the piezoelectric sandwich structure are expressed as:

$$\begin{aligned} \rho_A &= \rho_b h_b + 2\rho_p h_p \\ D_A &= D_b + \frac{2E_p}{3(1-\mu_p^2)}[(\frac{h_b}{2}+h_p)^3 - (\frac{h_b}{2})^3] \end{aligned} \tag{3}$$

here, $D_b = \frac{E_b h_b^3}{12(1-\mu_b^2)}$ is the flexural rigidity of the host plate and E_b, μ_b denote the Young's modulus and the Poisson's ratio of the host plate respectively; ρ_b and ρ_p are the densities of the host plate and the piezoelectric patches respectively.

In the third step, the effective area density and effective flexural rigidity of the entire shunted piezoelectric cell are derived, they are expressed as [28]:

$$\begin{aligned} \rho_{eff} &= \chi\rho_A + (1-\chi)\rho_b h_b \\ D_{eff} &= \frac{D_A D_b}{\chi D_A + (1-\chi)D_b} \end{aligned} \tag{4}$$

here, $\chi = (l_p/l_b)^2$ is the ratio of the surface covered by the piezoelectric patch to the surface of the unit cell.

In the last step, the effective refractive index of flexural wave incident from the background plate into the shunted piezoelectric cell is obtained:

$$n_{eff} = (\frac{\rho_{eff} D_b}{\rho_b h_b D_{eff}})^{1/4} \tag{5}$$

With the relationship in equation (5), a piezo-lens is designed in three steps. Firstly, the parameters α and β in the refractive index function in equation (1) are chosen to design the location of the focal point. Then, the required refractive index for each row of piezoelectric cell in the lens zone is obtained by substituting the central y coordinate of each row into equation (1). Lastly, the required refractive index for each row is fulfilled by choosing the NC value according to equation (5).

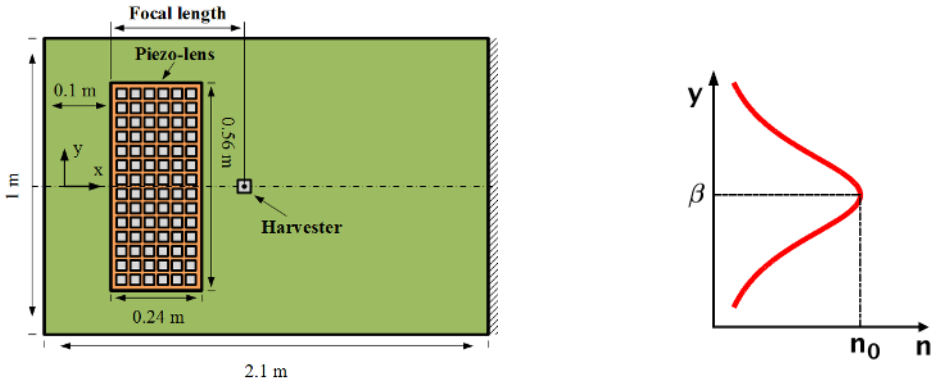

(a) (b)

Figure 1: (a) The harvesting system with piezo-lens and (b) the gradient variation profile of the refractive index $n(y)$.

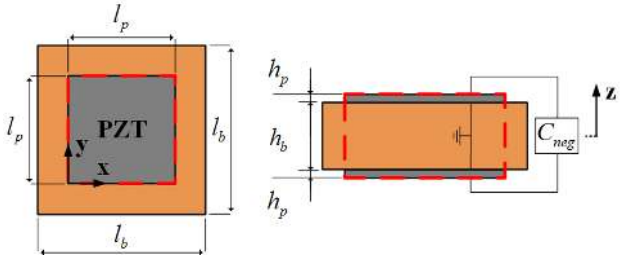

Figure 2: Top and side view of one unit shunted piezoelectric cell

2.2. The second part: a harvester

The harvester (namely the harvesting device) is located at the designed focal point to yield energy from the focused waves. The harvesting device is composed of a piezoelectric patch bonded on the upper surface of the plate and a connected energy extraction circuit. A standard DC device and two SSHI-based devices are analyzed in this paper, their topologies and the control strategies of the SSHI-based devices in transient wave energy harvesting are introduced hereinafter.

The DC device involves a rectifier to convert the voltage of the transducer to a DC form, and a capacitance C_s to store the harvested energy, as depicted in figure 3(a). In that figure, the piezoelectric patch is equivalently represented by a current source $I_{eq}(t)$ and a capacitance C_h with the value equal to the blocked intrinsic capacitance (i.e. the capacitance when the patch is under constant strain condition) [14]. The rectifier is assumed to be perfect. Thus, when the absolute value of $V_h(t)$ is larger than or equal to the output voltage $V_{C_s}(t)$, the rectifier conducts, the storage capacitance is charged. Under this circumstance, the harvesting circuit is governed by the equations below:

$$\dot{V}_h(t) = -\frac{\dot{Q}_h(t)}{C_s}, \; V_{C_s}(t) = |V_h(t)| \tag{6}$$

On the other hand, when the absolute value of $V_h(t)$ is smaller than the output voltage $V_{C_s}(t)$, the rectifier is blocked, no charge will flow to the storage capacitance, the piezoelectric element is under open-circuit condition:

$$\dot{V}_h(t) = \frac{\dot{I}_{eq}(t)}{C_h},\ \dot{V}_{C_s}(t) = 0 \tag{7}$$

in which, the exact expression of I_{eq} is given in subsection 3.2.

The SSHI-based harvesting devices are obtained by integrating a SSHI interface into the DC one shown in figure 3(a). In the first SSHI-based device, the SSHI interface, consists of a switch S and an inductor L, is in parallel to the piezoelectric patch as illustrated in figure 3(b). It is called parallel SSHI-DC (P-SSHI-DC) device in this paper. The control law of the switch is similar to the one used in steady state cases. At most of the time, the switch is opened, the device works just like a standard DC one. The switch is triggered at the time t_i when the current I_{eq} is null (namely, the voltage of the piezoelectric patch is a local maximum or minimum). It is kept closed for a very short period of time, corresponding to a half of the period of the oscillating circuit: $\Delta t = \pi\sqrt{LC_h}$. An inversion quality factor Q_I [10] is used to describe the energy loss mainly caused by the inductor in the SSHI interface (note that in some papers [17, 18], the voltage inversion coefficient $\gamma = e^{(-\frac{\pi}{2Q_I})}$ is used). In the simulations, this loss is taken into account by adding a resistive part $R_L = \frac{1}{Q_I}\sqrt{\frac{L}{C_h}}$ with the inductor. Thus the governing equations for the circuit during the inversion process are:

$$\begin{aligned} L\ddot{Q}_h(t) + R_l\dot{Q}_h(t) + \frac{Q_h(t)}{C_h} &= 0 \\ \dot{V}_h(t) = \frac{\dot{Q}_h(t)}{C_h},\ \dot{V}_{C_s}(t) &= 0 \end{aligned} \tag{8}$$

The second SSHI-based device contains a SSHI interface in series with the piezoelectric patch, as shown in figure 3(c). This device is called series SSHI-DC (S-SSHI-DC) device here. At most of the time, the piezoelectric element is under open-circuit condition. Different from the steady state cases [11, 12], the switch is closed when I_{eq} is null and $|V_h(t_i)| \geq V_{C_s}(t_i)$, the duration is $\Delta t = \pi\sqrt{L\frac{C_hC_s}{C_h+C_s}}$. An inversion quality factor Q_I is also used to take into account the loss of the switch interface in this case, accordingly a resistive part $R_l = \frac{1}{Q_I}\sqrt{L\frac{C_h+C_s}{C_hC_s}}$ is added to the inductor. The inversion process is governed by the equations below:

$$\begin{aligned} L\ddot{Q}_h(t) + R_l\dot{Q}_h(t) + \frac{Q_h(t)}{C_hC_s/(C_h+C_s)} &= 0 \\ \dot{V}_h(t) = \frac{\dot{Q}_h(t)}{C_h},\ V_l(t) &= -L\ddot{Q}_h(t) - R_l\dot{Q}_h(t) \\ V_{C_s}(t) &= |V_h(t) - V_l(t)| \end{aligned} \tag{9}$$

in which, $V_l(t)$ is the voltage difference between the two ends of the inductor.

3. Numerical models

3.1. Full finite element models

To study performances of the harvesting system, finite element (FE) models of piezoelectric systems are developed. In the FE models, the structures are discretized by 3D quadratic

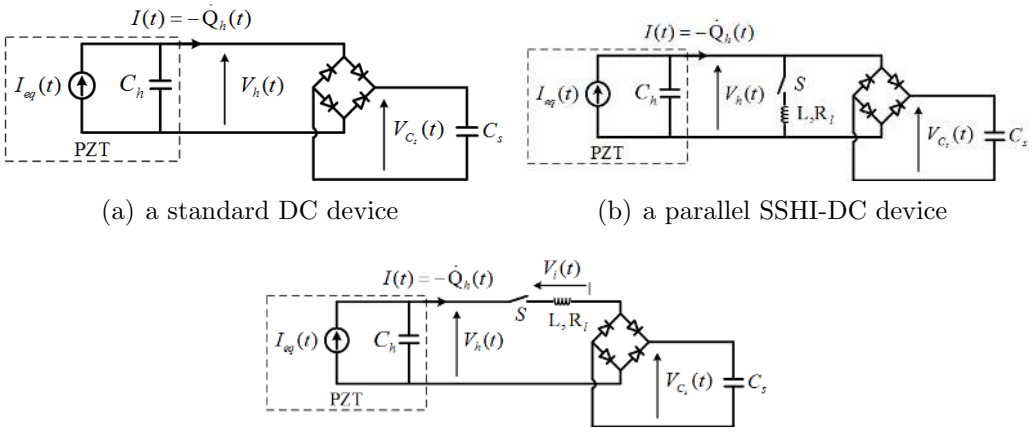

(a) a standard DC device

(b) a parallel SSHI-DC device

(c) a series SSHI-DC device

Figure 3: Tested harvesting devices.

Lagrange elements. Each of the nodes corresponding to the piezoelectric patches has three mechanical degrees of freedom (DOFs) and a voltage DOF. The equilibrium equations for the discretized fully coupled piezoelectric system are:

$$\begin{aligned} \boldsymbol{M}_{dd}\ddot{\boldsymbol{d}} + \boldsymbol{K}_{dd}\boldsymbol{d} + \boldsymbol{K}_{dV}\boldsymbol{V} &= \boldsymbol{F} \\ -\boldsymbol{K}_{dV}^{T}\boldsymbol{d} + \boldsymbol{K}_{VV}\boldsymbol{V} &= \boldsymbol{Q} \end{aligned} \tag{10}$$

here, $\boldsymbol{d}$ and $\boldsymbol{V}$ represent the structural and voltage DOFs, respectively; $\boldsymbol{F}$ and $\boldsymbol{Q}$ are the mechanical forces and charges respectively.

The equations in (10) are rewritten under following considerations: (i) the voltage DOFs in the piezoelectric patches can be partitioned into DOFs inside the patches, DOFs on the free electrodes of the patches and DOFs on the bonding surfaces; (ii) the voltage DOFs on the bonding surfaces are grounded, thus the corresponding equations and columns are directly removed; (iii) there is no charge source inside the piezoelectric patches, thus the internal voltage DOFs can be eliminated by exact static condensation; (iv) in the system, the piezoelectric patches are connected with different circuits - the patches constituting the piezo-lens are connected with NC circuits and the patch for harvesting is connected with one of the circuit illustrated in figure 3, therefore, the DOFs on the free electrodes are further separated into DOFs corresponding to the patches in the piezo-lens and DOFs of the patch for harvesting; (v) as the DOFs on one electrode have identical voltages, the voltage DOFs on the free electrode of each piezoelectric patch are reduced such that only one master voltage DOF remains on the free electrode per patch. Consequently, the governing equations can be rewritten as below:

$$\begin{bmatrix} \mathbf{M_{dd}} & 0 & 0 \\ 0 & 0 & 0 \\ 0 & 0 & 0 \end{bmatrix} \begin{Bmatrix} \ddot{\boldsymbol{d}} \\ \ddot{\boldsymbol{V}}_L \\ \ddot{\boldsymbol{V}}_h \end{Bmatrix} + \begin{bmatrix} \boldsymbol{H}_{dd} & \mathbf{H}_{dL} & \mathbf{H}_{dh} \\ -\mathbf{H}_{dL}^{T} & \mathbf{C}_L & 0 \\ -\mathbf{H}_{dh}^{T} & 0 & \mathbf{C}_h \end{bmatrix} \begin{Bmatrix} \boldsymbol{d} \\ \boldsymbol{V}_L \\ \boldsymbol{V}_h \end{Bmatrix} = \begin{Bmatrix} \boldsymbol{F} \\ \boldsymbol{Q}_L \\ \boldsymbol{Q}_h \end{Bmatrix} \tag{11}$$

in which, the matrices $\boldsymbol{C}_L$ and $\boldsymbol{C}_h$ are diagonal, each of their diagonal elements represents the blocked intrinsic capacitance of a piezoelectric patch; $\boldsymbol{V}_L$, $\boldsymbol{V}_h$ are the master DOFs on the free electrodes of the patches in the lens and the patch for harvesting, respectively; $\boldsymbol{Q}_L$,

$\boldsymbol{Q}_h$ are the charges flowing to the patches in the lens and patch for harvesting respectively. More details about above process could be found in the Appendix or [29].

3.2. Model reduction

Instead of solving the full finite element model above, which has a large number of DOFs, a reduced model is used. For the sake of simplicity, let:

$$\begin{aligned} \boldsymbol{H}_{dV} &= [\boldsymbol{H}_{dL},\ \boldsymbol{H}_{dh}],\ \boldsymbol{V} = [\boldsymbol{V}_L,\ \boldsymbol{V}_h]^T \\ \boldsymbol{Q} &= [\boldsymbol{Q}_L,\ \boldsymbol{Q}_h]^T,\ \boldsymbol{C}_{Lh} = \begin{bmatrix} \boldsymbol{C}_L & 0 \\ 0 & \boldsymbol{C}_h \end{bmatrix} \end{aligned} \tag{12}$$

Using these notations and equations (11), the governing equations in time domain are written as:

$$\boldsymbol{M}_{dd}\ddot{\boldsymbol{d}} + \boldsymbol{H}_{dd}\boldsymbol{d} + \boldsymbol{H}_{dV}\boldsymbol{V} = \boldsymbol{F} \tag{13a}$$

$$-\boldsymbol{H}_{dV}^T\dot{\boldsymbol{d}} + \boldsymbol{C}_{Lh}\dot{\boldsymbol{V}} = \dot{\boldsymbol{Q}} \tag{13b}$$

Equation (13b) and the following equations (17b), (20b) represent the Kirchhoff's current law which must be satisfied at the joints where circuits are connected with the piezoelectric patches.

The reduced model is obtained through a transformation between the displacement $\boldsymbol{d}$ and a set of modal coordinates $\boldsymbol{\eta}$:

$$\boldsymbol{d} = \boldsymbol{\Phi}\boldsymbol{\eta} \tag{14}$$

in which, $\boldsymbol{\Phi} = [\phi_1, \phi_2, ..., \phi_m]$. ϕ_i is the ith natural mode of the piezoelectric system under short-circuit condition with specific homogeneous Dirichlet boundaries, it is obtained by solving the following eigenvalue problem:

$$(-\omega_i^2\boldsymbol{M}_{dd} + \boldsymbol{H}_{dd})\phi_i = 0 \tag{15}$$

here, ω_i is the corresponding natural frequency. The modes are mass-normalized, resulting in:

$$\boldsymbol{\Phi}^T\boldsymbol{M}_{dd}\boldsymbol{\Phi} = \boldsymbol{I},\ \boldsymbol{\Phi}^T\boldsymbol{H}_{dd}\boldsymbol{\Phi} = \boldsymbol{\Lambda} = diag(\omega_i^2) \tag{16}$$

Using equations (14) and (16), the governing equations (13) are represented in modal coordinates as:

$$\ddot{\boldsymbol{\eta}} + \boldsymbol{\Lambda}\boldsymbol{\eta} + \boldsymbol{\Phi}^T\boldsymbol{H}_{dV}\boldsymbol{V} = \boldsymbol{\Phi}^T\boldsymbol{F} \tag{17a}$$

$$-\boldsymbol{H}_{dV}^T\boldsymbol{\Phi}\dot{\boldsymbol{\eta}} + \boldsymbol{C}_{Lh}\dot{\boldsymbol{V}} = \dot{\boldsymbol{Q}} \tag{17b}$$

Only the first m modes in modal matrix $\boldsymbol{\Phi}$ will be retained, and the number is much smaller than that of the system's DOFs. Thus, the number of equations in (17) is largely reduced.

However, the reduced model in equations (17) can't accurately describe the piezoelectric behaviors of the system [30] since the truncation of the higher order modes will lead to a static

reduction error [29]. This static error will cause a non-negligible error of the electrostatic voltage relative to the full model's as indicated below:

$$\boldsymbol{T}^e_{err} = \boldsymbol{T}^e_f - \boldsymbol{T}^e_r = \boldsymbol{H}^T_{dV}(\boldsymbol{H}^{-1}_{dd} - \boldsymbol{\Phi}\boldsymbol{\Lambda}^{-1}\boldsymbol{\Phi}^T)\boldsymbol{H}_{dV} \tag{18}$$

here, $\boldsymbol{T}^e_f$ and $\boldsymbol{T}^e_r$ are the electrostatic transfer matrices between $\boldsymbol{V}$ and $\boldsymbol{Q}$ of the full and reduced models, respectively.

To obtain more accurate voltage responses, the reduced model is corrected by modifying the blocked intrinsic capacitance matrix $\boldsymbol{C}_{Lh}$. The voltage responses are corrected by guaranteeing that the voltage outputs $\boldsymbol{V}(i)$ of the i^{th} piezoelectric patch in the corrected reduced model and the full model are consistent when a same static electric input $\dot{\boldsymbol{Q}}(i)$ is applied to this patch. According to equations (13) and (17), such requirement is fulfilled by modifying the capacitance matrix $\boldsymbol{C}^*_{Lh}$ in the corrected model as:

$$\boldsymbol{C}^*_{Lh} = \begin{bmatrix} \boldsymbol{C}^*_L & 0 \\ 0 & \boldsymbol{C}^*_h \end{bmatrix} = diag(\boldsymbol{H}^T_{dV}(\boldsymbol{H}^{-1}_{dd} - \boldsymbol{\Phi}\boldsymbol{\Lambda}^{-1}\boldsymbol{\Phi}^T)\boldsymbol{H}_{dV}) + \boldsymbol{C}_{Lh} \tag{19}$$

$\boldsymbol{C}^*_{Lh}$ is still a diagonal matrix, the diagonal terms of $\boldsymbol{C}^*_L$ and $\boldsymbol{C}^*_h$ represent the modified blocked intrinsic capacitances of corresponding patches. The corrected reduced model is obtained by replacing the $\boldsymbol{C}_{Lh}$ in equation (17b) with $\boldsymbol{C}^*_{Lh}$:

$$\ddot{\boldsymbol{\eta}} + \boldsymbol{\Lambda}\boldsymbol{\eta} + \boldsymbol{\Phi}^T\boldsymbol{H}_{dV}\boldsymbol{V} = \boldsymbol{\Phi}^T\boldsymbol{F} \tag{20a}$$

$$-\boldsymbol{H}^T_{dV}\boldsymbol{\Phi}\dot{\boldsymbol{\eta}} + \boldsymbol{C}^*_{Lh}\dot{\boldsymbol{V}} = \dot{\boldsymbol{Q}} \tag{20b}$$

The structural damping is taken into account by introducing a constant viscous damping coefficient $2\xi\omega_i$ into each remained mode. The NC circuits are connected to the piezoelectric patches through the following relation:

$$\dot{\boldsymbol{Q}}_L(t) = -\boldsymbol{C}_{\boldsymbol{neg}}\dot{\boldsymbol{V}}_L(t) \tag{21}$$

The DC and SSHI-based circuits are implemented in the corrected reduced models through equations (6) to (9). Note that, in the equivalent model of the piezoelectric patch for harvesting, the current source is $I_{eq}(t) = \boldsymbol{H}^T_{dV}\boldsymbol{\Phi}\dot{\boldsymbol{\eta}}(t)$ and the blocked intrinsic capacitance is the modified one C^*_h.

4. Numerical results

In the simulations, the dimensions of the piezo-lens and host plate are illustrated in figure 1(a). The geometry parameters of the piezoelectric cells and piezoelectric patch for harvesting are given in table 1, meanings of the symbols used in table 1 are given in figure 2. The Young's modulus, Poisson's ratio and density of the aluminum plate are $E_b = 70\ Gpa$, $\mu_b = 0.3$ and $\rho_b = 2700\ kg/m^3$, respectively. The material parameters for the PZTs are listed in table 2. The plate is clamped at the right end side and a 10-period Hanning-windowed tone burst excitation with central frequency 2000 Hz is applied at the left end side to generate transient waves. The excitation is a line transverse force, its waveform and spectrum are illustrated in figure 4. Modes that have natural frequencies smaller than five times of the maximum frequency of interest are remained in the reduced model; a small damping coefficient $\xi = 0.001$ is used to minimize the influence of the structural damping on

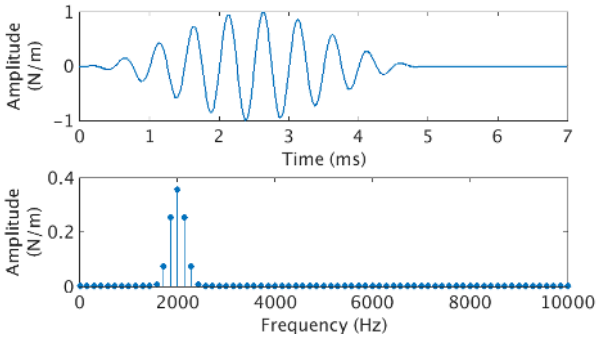

Figure 4: The applied tone burst excitation.

Table 1: Geometry parameters

	l_b	h_b	l_p	h_p
piezoelectric cell	0.04 m	0.005 m	0.035 m	0.001 m
piezoelectric patch for harvesting	\	\	0.05 m	0.001 m

the wave propagation. The classical Runge-Kutta method is used to solve the ODEs using a fixed time step equal to $1 \times 10^{-6} s$.

The piezo-lens' parameters are chosen as $\alpha = \pi/0.6,\ \beta = 0$, and the harvester is mounted at the corresponding focal point, which is located on the $y = 0$ line (namely the central axis) with a distance of 0.06 m from the right boundary of the lens. (Note that the focal lenght is 0.3 m counting from the left boundary.) These values are chosen because the energy will be more better concentrated if the focal point of the piezo-lens is designed on the central axis and close to the lens boundary [25].

4.1. Comparison between the standard DC and SSHI-based devices

The standard DC and SSHI-based harvesting devices have been well studied in steady state, however lack of knowledge of their applications in transient wave cases could be found. Thus first of all, the performances of the systems with these devices in transient wave energy harvesting are studied. The piezo-lens is applied in these studies. To assess the harvesting performances, two metrics are used. The first one is the harvested energy, which indicates how much energy can be yielded when a transient wave package passes through the harvester, it is the maximum energy that stored in the storage capacitance of the harvesting device:

$$E_{har} = max(\frac{1}{2} C_s V_{C_s}^2(t)) \tag{22}$$

The second one is the harvesting efficiency, it is defined as [31]:

$$\eta_E = \frac{E_{har}}{E_{input}} \tag{23}$$

in which, E_{input} is the total input energy introduced by the excitation. The efficiency indicates how much a harvesting system can convert the input mechanical energy (E_{input}) into

Table 2: Material parameters of PZT26

Symbol	Value	Property
$S_{11}^E = S_{22}^E, S_{33}^E$ $S_{12}^E, S_{13}^E = S_{23}^E$ $S_{44}^E = S_{55}^E, S_{66}^E$	$1.30 \times 10^{-11}, 1.96 \times 10^{-11}$ (Pa^{-1}) $-4.35 \times 10^{-12}, -7.05 \times 10^{-12}$ (Pa^{-1}) $3.32 \times 10^{-11}, 3.47 \times 10^{-11}$ (Pa^{-1})	Compliance matrix under constant electric field
$d_{31} = d_{32}$ d_{33} $d_{24} = d_{15}$	-1.28×10^{-10} (C/N) 3.28×10^{-10} (C/N) 3.27×10^{-10} (C/N)	Piezoelectric matrix
ρ	7700 (kg/m^3)	Density
$\varepsilon_{11}^\sigma = \varepsilon_{22}^\sigma$, ε_{33}^σ	$1190\varepsilon_0$, $1330\varepsilon_0$	Dielectric permittivity under constant stress

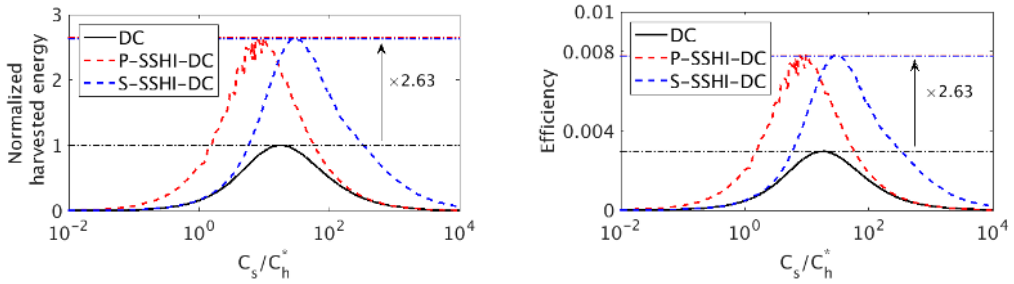

(a) harvested energy (b) efficiency

Figure 5: Performances of the harvesting system with piezo-lens when different devices are used, $Q_I = 3$.

the output electric one (E_{har}). This metric is a useful criterion to compare the harvesting performances of systems with different configurations and/or under different operating conditions.

The performances of systems with different harvesting devices are compared in figure 5. In the simulations in figure 5 and those hereinafter, the inversion quality factor Q_I of the SSHI-based device is equal to 3. Q_I indicates the energy loss caused by the harvesting circuit, typically a larger value of it means less energy loss [10]. Q_I mainly depends on the involved piezoelectric material, the switch and the inversion inductance, its real value can only be obtained experimentally, herein the value of it is chosen according to the results in [10]. From figure 5 it can be seen that the harvested energy and efficiency strongly depend on the storage capacitance, and the optimal capacitances corresponding to the maximum harvested energy and the maximum efficiency are nearly the same for each device. In addition, when the devices are all working at optimal conditions, the two SSHI-based devices have almost equal performances, and they both harvest 2.6 times more energy than the DC device and also have 2.6 times better efficiency.

To gain more insights into the harvesting performances of the systems with DC or SSHI-based devices, the typical waveforms and the converted power are compared in figure 6. The meanings of V_h, I_{eq} and V_{C_s} are given in figure 3; the converted power is the product of V_h and I_{eq}, positive it represents the amount of power converted from mechanical to electrical, and negative it means the contrary. In the simulations in figure 6, the storage capacitances are all set as $C_s = 30C_h^*$ to guarantee an acceptable performance for all the devices according

to the results in figure 5. To facilitate the comparison, the maximum V_{C_s} in the DC case is normalized to unit, and all the other voltages are normalized according to this value; a similar normalization process is used to deal with the converted power.

When the transient wave package reaches the harvester, the charges begin to accumulate in the storage capacitance; the accumulation stops after the main part of the package passes through the harvester. The charges accumulated in the storage capacitance are converted from strain energy by the piezoelectric transducer, it can be seen that the SSHI-based devices can promote the conversion of power from mechanical to electrical part but suppress the contrary, thus they can harvest more energy than the DC device. It can also be observed that when the SSHI-based devices are used, the waveforms of I_{eq} are distorted. I_{eq} depends directly on the strains of the piezoelectric patches, which are caused by the waves in the media, the distortions indicate that the harvesting processes in those cases could have non-negligible influences on the wave propagation at the location where the harvester is mounted. Since the switch is trigged at the time when $I_{eq} = 0$, the distortions result in multiple inversions, which cause the fluctuation of the harvesting performance as revealed in figure 5.

4.2. Effects of piezo-lens on transient waves and harvesting

It is demonstrated in [25] that the piezo-lens can focus harmonic waves near the designed focal point in a large frequency band, thus it is expected that the piezo-lens could also focus transient waves if the main frequency components of the waves are within the effective frequency band of the piezo-lens, and harvesting at the designed focal point can yield improved energy. This expectation is verified in this subsection.

According to the results in [25], the piezo-lens used in this paper is effective from about 100 Hz to 8000 Hz. Thus the major frequency components of the waves generated by the excitation in figure 4 are totally within the effective frequency band. Firstly to study the effect of the piezo-lens on transient waves, the harvester is removed from the system since its presence at the focal point will make the energy concentration effect less obvious. The instantaneous transverse displacement w_f at the designed focal point and input power are shown in figure 7(a). The results corresponding to the case without lens are also given as references, the maximum amplitudes of the transverse displacement and input power in this case are both normalized to unity. The piezo-lens will reflects a part of the incident waves and these reflected waves will interact with the excitation forces, thus the input power is a little bit reduced when the piezo-lens is active. Even though with this reduction of input power, the maximum amplitude of w_f is improved. This result indicates that the transient waves are focused by the lens. To further verify the focusing effect, the transverse displacement of the host plate at the time corresponding to the maximum amplitude of w_f is depicted in figure 7(b) for the case without piezo-lens and in figure 7(c) for the case with piezo-lens. From the comparison, it can be clearly observed that the transient waves are focused near the designed focal point.

Figure 8 compares the harvesting performances between the cases with and without piezo-lens. When the piezo-lens is used and due to the focusing effect demonstrated above, the maximum harvested energy is enhanced about 2.5 times no matter which kind of harvester is used. The input power is reduced when the piezo-lens is applied, consequently the maximum harvesting efficiency is improved about 3 times for each device as illustrated in figure 8(b).

In the above studies, it is verified that the piezo-lens can enhance the harvested energy from transient waves when the harvester is located at the designed focal point. However in the studies in figure 7 the harvester is removed from the system, it is not clear that

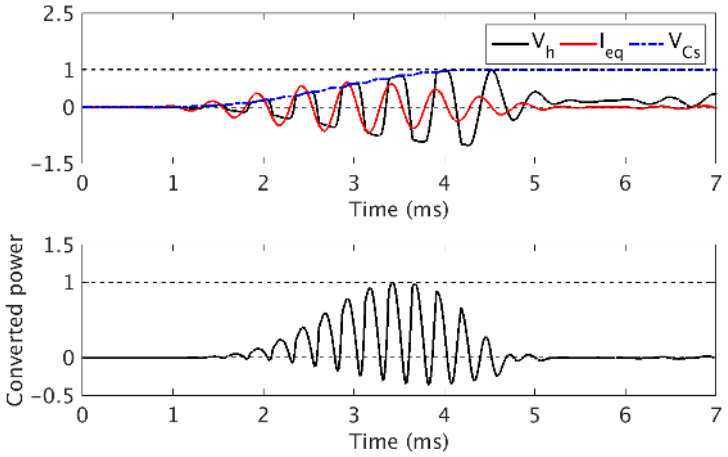

(a) standard DC, $C_s = 30C_h^*$

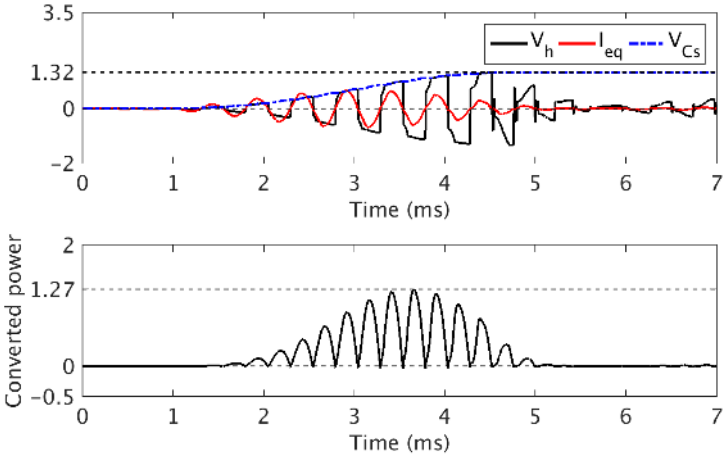

(b) P-SSHI-DC, $Q_I = 3,\ C_s = 30C_h^*$

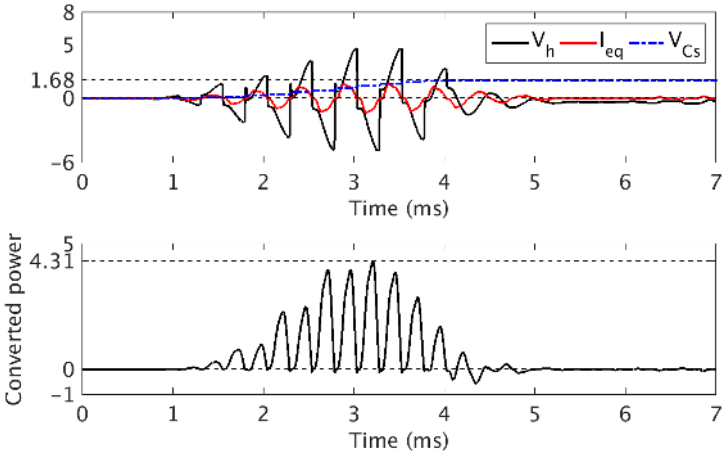

(c) S-SSHI-DC, $Q_I = 3,\ C_s = 30C_h^*$

Figure 6: Typical waveforms and converted energy when DC and SSHI-based devices are used to harvest energy from transient waves.

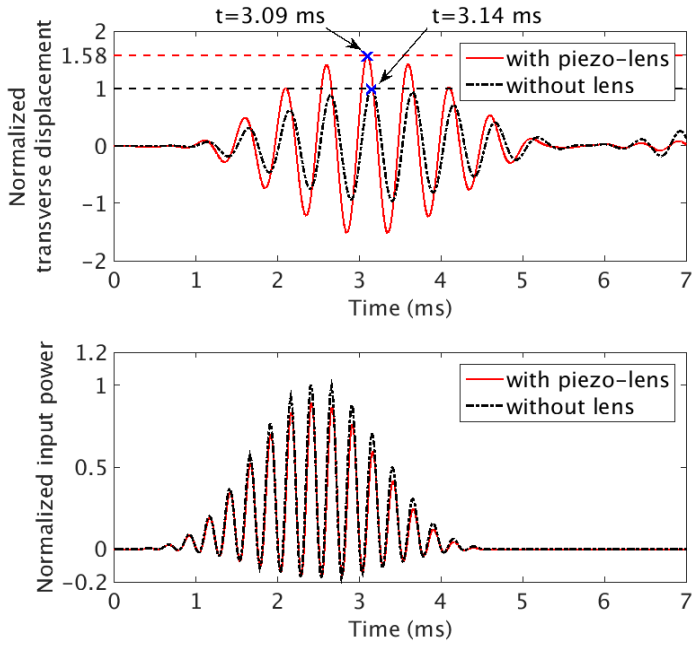

(a) upper: normalized transverse displacement at the focal point; lower: normzlaized input powers

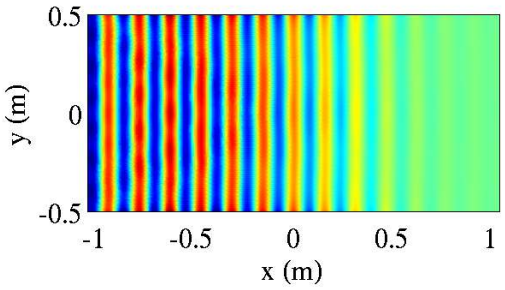

(b) transvers dispalcement of the plate without lens at $t = 3.14\ ms$.

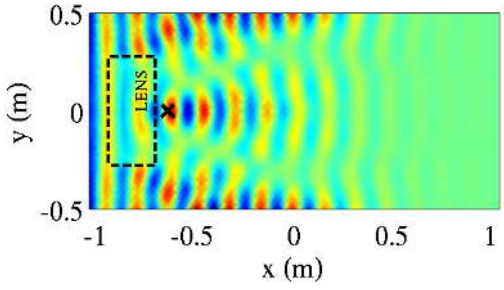

(c) transvers dispalcement of the plate with piezo-lens at $t = 3.09\ ms$.

Figure 7: Focusing transient waves.

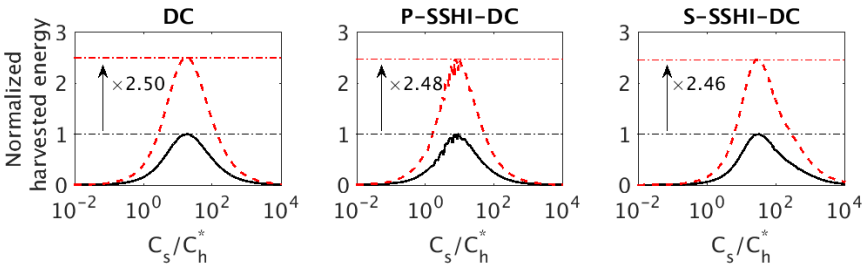

(a) harvested energy

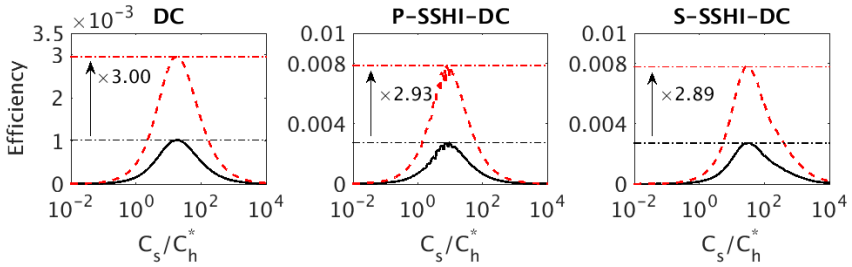

(b) efficiency

Figure 8: Comparison of the performances between the cases with and without piezo-lens. – – –: with piezo-lens; ——: without lens. $Q_I = 3$.

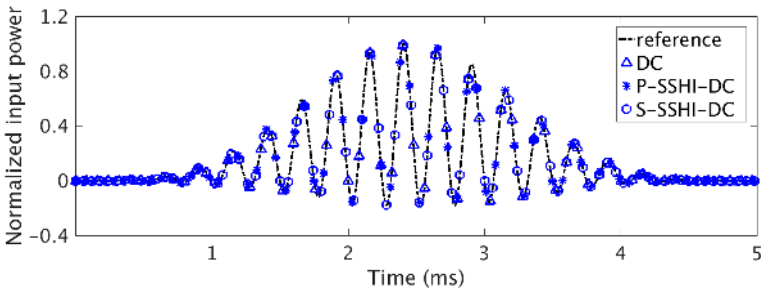

Figure 9: Comparison of the input power when different devices are used to harvest the transient waves, the storage capacitance for each device is optimal, the reference input power refers to the case without any harvesting device.

whether the placement of the harvester near the piezo-lens will has significant influence on the location where the waves are concentrated. This is important since if the influence is non-negligible, the designed focal point may not be the optimal place for harvesting. The energy concentration location only depends on the incident waves when the parameters of the piezo-lens are specified [25], thus if the harvester has negligible effect on the excitation source, it will not affect the incident waves and the consequent energy concentration location. To study the influence of the harvester on the transient source, the instantaneous input power is used as a criterion. Figure 9 shows the input power induced by the transient excitation when different harvesters are used in the harvesting system. In these studies, the storage capacitance for each harvester is chosen to make the output energy maximum. The reference input power in the figure refers to the case without any harvesting device, and the maximum of it is normalized to unity. It can be observed that the harvester do not affect the input power, accordingly they won't influence the generated transient waves and the energy concentration location.

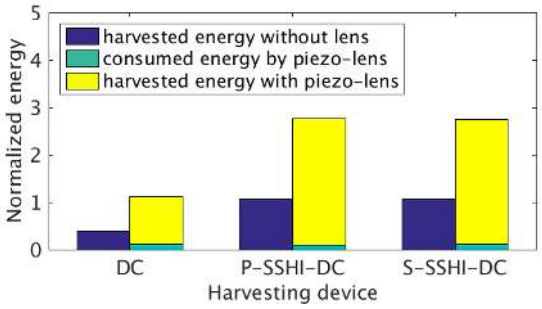

Figure 10: Comparison of the consumed and harvested energy in the harvesting system, the storage capacitance for each device is optimal, $Q_I = 3$.

4.3. Energy balance

Since the NC circuits in the piezo-lens are active elements and they need to be powered, it is also important to consider the energy balance of the harvesting system. In the piezo-lens, the NC circuits need to stiffen the structure. To realize such effect, the circuits should be fully reactive [32], namely, they doesn't dissipate any energy. Thus, the active energy consumed by the NC circuit in a time interval from t_1 to t_2 is expressed as:

$$E_{C_{neg}} = \int_{t_1}^{t_2} V_{neg}(t) I_{neg}(t) = \frac{1}{2} C_{neg}(V_{neg}^2(t_2) - V_{neg}^2(t_1)) \tag{24}$$

For the transient wave cases here, the consumed energy is estimated in the interval between the time when the transient wave package first arrives at the piezo-lens and the time when the package leaves the lens. Figure 10 compares the consumed and harvested energy in the cases with different devices. The storage capacitance for each device is optimal (namely the output energy is maximum); the harvested energy of the system with piezo-lens and DC device is normalized to unity. When the piezo-lens is applied in harvesting systems, it is observed that the amount of consumed energy is really small compared with the harvested one, 11% with the DC device and less than 4% with the SSHI-based devices. Thus even though we take into account the energy consumed by the piezo-lens, the harvesting systems incorporating the piezo-lens still can yield considerably improved energy compared with the cases without piezo-lens.

4.4. Practical application considerations

In previous sections, performance of the harvesting systems are verified in ideal situations with very small structural damping ($\xi = 0.001$) and neglected forward voltages of diodes. In this section, influences of these factors on harvesting performance are considered, and applicability of the harvesting systems is discussed. In new examples, the structural damping is given as $\xi = 0.05$, the forward voltage of each diode is 0.6 V, the inversion quality factor Q_I for SSHI interface is chosen as 5.6 according to the experimental results in [10], and the storage capacitance C_s for each harvester is chosen to make the output energy maximum, i.e., $C_s = 14C_h^*$ for the DC harvester, $C_s = 7.4C_h^*$ for the P-SSHI-DC harvester and $C_s = 30C_h^*$ for the S-SSHI-DC harvester ($C_h^* = 22.0\ nF$).

Figure 11 shows the waveforms of displacements and voltages in harvesting systems incorporating a piezo-lens. The measure location of the displacement is the left-bottom corner on the upper surface of the piezoelectric patch for harvesting. It can be observed that even

though the maximum amplitude of the mechanical response of the patch is only micrometer-scale, the harvesting systems are adequate to yield energy from the transient waves. It is noted here that the fast switch actions illustrated in figure 11(b) and 11(c) perhaps are difficult to obtain in piezoelectric mechanical systems. However, the piezo-lens can work at lower frequencies as long as the wavelengths are smaller than the characteristic length of the lens [25]. In those cases, the switch actions could be more realistic.

The improvement of harvesting performance by using piezo-lens in these new cases are illustrated in figure 12, in which, the mean power P_1 for the case without lens and the mean net power P_2 for the case with piezo-lens are defined as:

$$P_1 = \frac{E_{har1}}{t_{har1}}, \quad P_2 = \frac{E_{har2} - E_{C_{neg}}}{t_{har2}} \tag{25}$$

here, E_{har1} and E_{har2} are the harvested energy obtained by equation (22), $E_{C_{neg}}$ is the consumed energy by the piezo-lens evaluated by equation (24), t_{har1} and t_{har2} are the charging duration of the storage capacitances (see figure 11). From figure 12, it can be seen that the piezo-lens is also very effective to improve the harvesting performance in these more realistic cases.

Indeed, to realize the harvesting systems, there are still challenges. The NC circuits required in the piezo-lens need to be totally reactive to stiffen the structure, but the existing circuits that could realize negative capacitance all contain resistive parts which more or less will dissipate some energy [33, 34], thus they are potentially not suitable to realize a piezo-lens. However, it is hopeful that approximate fully reactive NC circuits could be achieved to reach the required stiffening effect in the coming future by optimizing the existing circuits (see [33]) or using synthetic circuits as proposed in [35]. Since the NC circuits for the piezo-lens are not determined at present, giving a rigorous energy balance analysis which takes into account the dissipated power is impossible, but it is logical to predict that the dissipated power by the piezo-lens could be very low since the NC circuits need to be (approximately) fully reactive. Besides, in some applications, the energy balance is not a critical issue. For example, a potential application of the harvesting systems is in Structural Health Monitoring (SHM) in large-scale structures. Sensors are sometimes embedded in structures at different locations in those cases, the maintenance is very difficult or even impossible when traditional batteries are used to power the sensors. Thus, the harvesting systems can be used to power these sensors. In these applications, the piezo-lens can be placed on the surfaces of structures thus it can be powered by traditional batteries rather than harvesters.

5. Conclusions

The combination of a piezo-lens with a harvester to obtain enhanced energy from transient traveling waves is studied. The standard DC, parallel SSHI-based and series SSHI-based harvesters are used. The SSHI interface can promote the conversion of the power from mechanical to electric part but suppress the contrary, accordingly the SSHI-based harvesters are more efficient than the standard DC one for harvesting energy from transient waves. The piezo-lens can focus transient waves near a designed focal point, thus placing the harvesters at that point can enhance the harvested energy about 2.5 - 3 times and improve the harvesting efficiency about 3 times as compared with the cases without lens. This improvement of harvesting performance is obtainable when the realistic damping effect of the host structure and the forward voltages of diodes are taken into account.

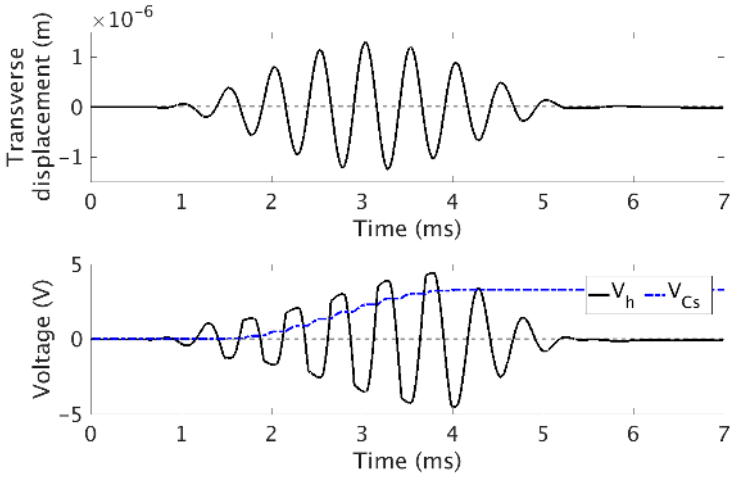

(a) standard DC, $C_s = 14C_h^*$

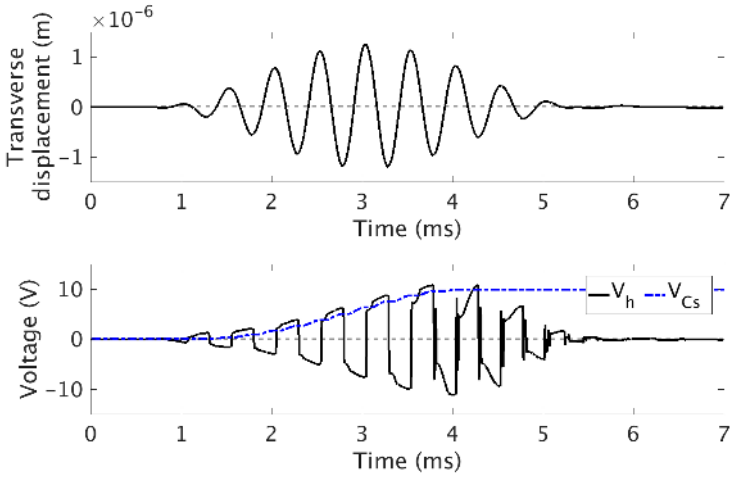

(b) P-SSHI-DC, $Q_I = 5.6,\ C_s = 7.4C_h^*$

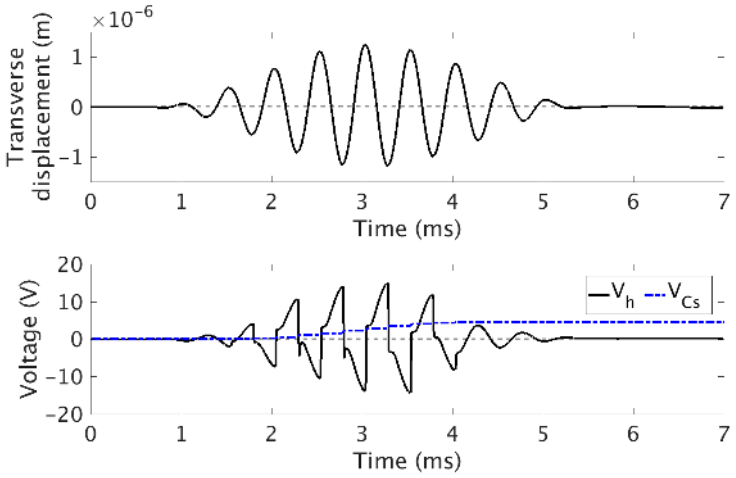

(c) S-SSHI-DC, $Q_I = 5.6,\ C_s = 30C_h^*$

Figure 11: Waveforms of transverse displacement and voltages when DC and SSHI-based devices are used to harvest energy from transient waves. The measure location of the displacement is the left-bottom corner on the upper surface of the piezoelectric patch for harvesting.

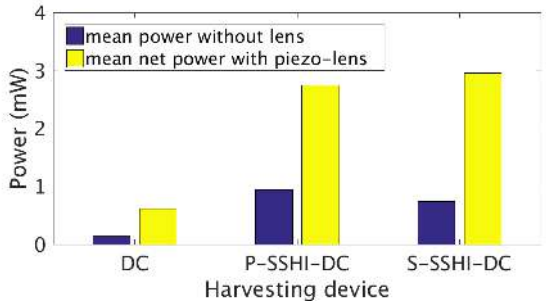

Figure 12: Comparison of the mean harvested power between the cases without and with piezo-lens.

Acknowledgement

The authors acknowledge Carnot Institute Ingénierie@Lyon for granting this study. The first author also thanks a scholarship provided by the China Scholarship Council.

Appendix: Outlines of the derivation of the fully coupled finite element models for piezoelectric systems

The potential DOFs in the piezoelectric patches are partitioned into DOFs inside the patches $\boldsymbol{V}_i$, DOFs on the free electrodes of the patches $\boldsymbol{V}_p$ and DOFs on the bonding surfaces $\boldsymbol{V}_g$. The potential DOFs on the bonding surfaces are grounded, thus the corresponding equations and columns are directly removed from the equations. Consequently, the governing equations in (10) are partitioned as below:

$$\begin{bmatrix} \mathbf{M_{dd}} & 0 & 0 \\ 0 & 0 & 0 \\ 0 & 0 & 0 \end{bmatrix} \begin{Bmatrix} \ddot{\boldsymbol{d}} \\ \ddot{\boldsymbol{V}}_i \\ \ddot{\boldsymbol{V}}_p \end{Bmatrix} + \begin{bmatrix} \boldsymbol{K}_{dd} & \mathbf{K}_{di} & \mathbf{K}_{dp} \\ -\mathbf{K}_{di}^T & \mathbf{K}_{ii} & \mathbf{K}_{ip} \\ -\mathbf{K}_{dp}^T & -\mathbf{K}_{ip}^T & \mathbf{K}_{pp} \end{bmatrix} \begin{Bmatrix} \boldsymbol{d} \\ \boldsymbol{V}_i \\ \boldsymbol{V}_p \end{Bmatrix} = \begin{Bmatrix} \boldsymbol{F} \\ \boldsymbol{Q}_i \\ \boldsymbol{Q}_p \end{Bmatrix} \tag{26}$$

Since there is no charge source inside the piezoelectric patches ($\boldsymbol{Q}_i = 0$), the internal DOFs $\boldsymbol{V}_i$ can be determined by exact static condensation from equation (26):

$$\boldsymbol{V}_i = -\boldsymbol{K}_{ii}^{-1}(-\boldsymbol{K}_{di}^T\boldsymbol{d} + \boldsymbol{K}_{ip}\boldsymbol{V}_p) \tag{27}$$

After the condensation, the system equations become:

$$\begin{bmatrix} \boldsymbol{M}_{dd} & 0 \\ 0 & 0 \end{bmatrix} \begin{Bmatrix} \ddot{\boldsymbol{d}} \\ \ddot{\boldsymbol{V}}_p \end{Bmatrix} + \begin{bmatrix} \boldsymbol{G}_{dd} & \boldsymbol{G}_{dp} \\ -\boldsymbol{G}_{dp}^T & \boldsymbol{G}_{pp} \end{bmatrix} \begin{Bmatrix} \boldsymbol{d} \\ \boldsymbol{V}_p \end{Bmatrix} = \begin{Bmatrix} \boldsymbol{F} \\ \boldsymbol{Q}_p \end{Bmatrix} \tag{28}$$

with

$$\begin{aligned} \boldsymbol{G}_{dd} &= \boldsymbol{K}_{dd} + \boldsymbol{K}_{di}\boldsymbol{K}_{ii}^{-1}\boldsymbol{K}_{di}^T \\ \boldsymbol{G}_{dp} &= \boldsymbol{K}_{dp} - \boldsymbol{K}_{di}\boldsymbol{K}_{ii}^{-1}\boldsymbol{K}_{ip} \\ \boldsymbol{G}_{pp} &= \boldsymbol{K}_{pp} + \boldsymbol{K}_{ip}^T\boldsymbol{K}_{ii}^{-1}\boldsymbol{K}_{ip} \end{aligned} \tag{29}$$

The DOFs $\mathbf{V}_p$ are further separated into DOFs corresponding to the patches in the piezo-lens $\boldsymbol{V}_{Lp}$ and DOFs of the patches for harvesting $\boldsymbol{V}_{hp}$:

$$\begin{bmatrix} \mathbf{M_{dd}} & 0 & 0 \\ 0 & 0 & 0 \\ 0 & 0 & 0 \end{bmatrix} \begin{Bmatrix} \ddot{\boldsymbol{d}} \\ \ddot{\boldsymbol{V}}_{Lp} \\ \ddot{\boldsymbol{V}}_{hp} \end{Bmatrix} + \begin{bmatrix} \boldsymbol{G}_{dd} & \mathbf{G}_{dL} & \mathbf{G}_{dh} \\ -\mathbf{G}_{dL}^T & \mathbf{G}_{LL} & 0 \\ -\mathbf{G}_{dh}^T & 0 & \mathbf{G}_{hh} \end{bmatrix} \begin{Bmatrix} \boldsymbol{d} \\ \boldsymbol{V}_{Lp} \\ \boldsymbol{V}_{hp} \end{Bmatrix} = \begin{Bmatrix} \boldsymbol{F} \\ \boldsymbol{Q}_{Lp} \\ \boldsymbol{Q}_{hp} \end{Bmatrix} \tag{30}$$

As the DOFs on one electrode have identical potentials, the potential DOFs on the free electrode of each piezoelectric patch are reduced such that only one master potential DOF remains per patch. The reduction is achieved by using an explicit transformation:

$$\begin{Bmatrix} \boldsymbol{V}_{Lp} \\ \boldsymbol{V}_{hp} \end{Bmatrix} = \begin{bmatrix} \boldsymbol{T}_L & 0 \\ 0 & \boldsymbol{T}_h \end{bmatrix} \begin{Bmatrix} \boldsymbol{V}_L \\ \boldsymbol{V}_h \end{Bmatrix} \tag{31}$$

here, $\boldsymbol{T} = \begin{bmatrix} \boldsymbol{T}_L & 0 \\ 0 & \boldsymbol{T}_h \end{bmatrix}$ is the transformation matrix, it represents the Null space of the linear transformation above, the nonzero terms in it is either 1 or -1.

Substituting equation (31) into equation (30) and then left multiplying the transposed transformation matrix yield the final fully coupled governing equations:

$$\begin{bmatrix} \mathbf{M_{dd}} & 0 & 0 \\ 0 & 0 & 0 \\ 0 & 0 & 0 \end{bmatrix} \begin{Bmatrix} \ddot{\boldsymbol{d}} \\ \ddot{\boldsymbol{V}}_{L} \\ \ddot{\boldsymbol{V}}_{h} \end{Bmatrix} + \begin{bmatrix} \boldsymbol{H}_{dd} & \mathbf{H}_{dL} & \mathbf{H}_{dh} \\ -\mathbf{H}_{dL}^T & \mathbf{C}_L & 0 \\ -\mathbf{H}_{dh}^T & 0 & \mathbf{C}_h \end{bmatrix} \begin{Bmatrix} \boldsymbol{d} \\ \boldsymbol{V}_{L} \\ \boldsymbol{V}_{h} \end{Bmatrix} = \begin{Bmatrix} \boldsymbol{F} \\ \boldsymbol{Q}_{L} \\ \boldsymbol{Q}_{h} \end{Bmatrix} \tag{32}$$

with

$$\begin{aligned} \boldsymbol{H}_{dd} = \boldsymbol{G}_{dd},\ \boldsymbol{H}_{dL} = \boldsymbol{G}_{dL}\boldsymbol{T}_L,\ \boldsymbol{H}_{dh} = \boldsymbol{G}_{dh}\boldsymbol{T}_h \\ \boldsymbol{C}_L = \boldsymbol{T}_L^T\boldsymbol{G}_{LL}\boldsymbol{T}_L,\ \boldsymbol{C}_h = \boldsymbol{T}_h^T\boldsymbol{G}_{hh}\boldsymbol{T}_h \\ \boldsymbol{Q}_L = \boldsymbol{T}_L^T\boldsymbol{Q}_{Lp},\ \boldsymbol{Q}_h = \boldsymbol{T}_h^T\boldsymbol{Q}_{hp} \end{aligned} \tag{33}$$

namely, equations (11) in section 3.1.

References

[1] M. Collet, M. Ouisse, and F. Tateo. Adaptive metacomposites for vibroacoustic control applications. *IEEE Sensors Journal*, 14(7):2145–2152, jul 2014.

[2] Minh Quyen Le, Jean-Fabien Capsal, Mickaël Lallart, Yoann Hebrard, Andre Van Der Ham, Nicolas Reffe, Lionel Geynet, and Pierre-Jean Cottinet. Review on energy harvesting for structural health monitoring in aeronautical applications. *Progress in Aerospace Sciences*, 79:1–11, 2015.

[3] Dibin Zhu, John Tudor, Steve Stephen P Beeby, Michael J Tudor, and Steve Stephen P Beeby. Strategies for increasing the operating frequency range of vibration energy harvesters: a review. *Measurement Science and Technology*, 21(2):022001, 2010.

[4] Nathan Jackson, Frank Stam, Oskar Z. Olszewski, Hugh Doyle, Aidan Quinn, and Alan Mathewson. Widening the bandwidth of vibration energy harvesters using a liquid-based non-uniform load distribution. *Sensors and Actuators A: Physical*, 2016.

[5] Liuyang Xiong, Lihua Tang, and Brian R. Mace. Internal resonance with commensurability induced by an auxiliary oscillator for broadband energy harvesting. *Applied Physics Letters*, 108(20):203901, 2016.

[6] Zhongsheng Chen, Yongmin Yang, Zhimiao Lu, and Yanting Luo. Broadband characteristics of vibration energy harvesting using one-dimensional phononic piezoelectric cantilever beams. *Physica B: Condensed Matter*, 410(1):5–12, 2013.

[7] Y. Fan, M. Collet, M. Ichchou, L. Li, O. Bareille, and Z. Dimitrijevic. A wave-based design of semi-active piezoelectric composites for broadband vibration control. *Smart Materials and Structures*, 25(5):055032, 2016.

[8] Liuxian Zhao, Stephen C Conlon, and Fabio Semperlotti. Broadband energy harvesting using acoustic black hole structural tailoring. *Smart Materials and Structures*, 23(6):065021, 2014.

[9] Daniel Guyomar and Mickaël Lallart. Recent progress in piezoelectric conversion and energy harvesting using nonlinear electronic interfaces and issues in small scale implementation. *Micromachines*, 2(2):274–294, 2011.

[10] Daniel Guyomar, Adrien Badel, Elie Lefeuvre, and Claude Richard. Toward energy harvesting using active materials and conversion improvement by nonlinear processing. *IEEE Transactions on Ultrasonics, Ferroelectrics, and Frequency Control*, 52(4):584–594, 2005.

[11] I C Lien, Y C Shu, W J Wu, S M Shiu, and H C Lin. Revisit of series-SSHI with comparisons to other interfacing circuits in piezoelectric energy harvesting. *Smart Materials and Structures*, 19(12):125009, 2010.

[12] E. Lefeuvre, A. Badel, C. Richard, L. Petit, and D. Guyomar. A comparison between several vibration-powered piezoelectric generators for standalone systems. *Sensors and Actuators, A: Physical*, 126(2):405–416, 2006.

[13] Y C Shu, I C Lien, and W J Wu. An improved analysis of the SSHI interface in piezoelectric energy harvesting. *Smart Materials and Structures*, 16(6):2253–2264, 2007.

[14] Junrui Liang and Wei-hsin Liao. Energy flow in piezoelectric energy harvesting systems. *Smart Materials and Structures*, 20(1):015005, 2011.

[15] Geffrey K. Ottman, Heath F. Hofmann, Archin C. Bhatt, and George A. Lesieutre. Adaptive piezoelectric energy harvesting circuit for wireless remote power supply. *IEEE Transactions on Power Electronics*, 17(5):669–676, 2002.

[16] Mickaël Lallart, Lauric Garbuio, Lionel Petit, Claude Richard, and Daniel Guyomar. Double synchronized switch harvesting (DSSH): A new energy harvesting scheme for efficient energy extraction. *IEEE Transactions on Ultrasonics, Ferroelectrics, and Frequency Control*, 55(10):2119–2130, 2008.

[17] Hui Shen, Jinhao Qiu, Hongli Ji, Kongjun Zhu, and Marco Balsi. Enhanced synchronized switch harvesting: a new energy harvesting scheme for efficient energy extraction. *Smart Materials and Structures*, 19(11):115017, 2010.

[18] Hui Shen, Hongli Ji, Jinhao Qiu, Yixiang Bian, and Dawei Liu. Adaptive synchronized switch harvesting: A new piezoelectric energy harvesting scheme for wideband vibrations. *Sensors and Actuators, A: Physical*, 226:21–36, 2015.

[19] H. G D Goyder and R. G. White. Vibrational power flow from machines into built-up structures, part I: Introduction and approximate analyses of beam and plate-like foundations. *Journal of Sound and Vibration*, 68(1):59–75, 1980.

[20] Y. Fan, M. Collet, M. Ichchou, L. Li, O. Bareille, and Z. Dimitrijevic. Energy flow prediction in built-up structures through a hybrid finite element/wave and finite element approach. *Mechanical Systems and Signal Processing*, 66-67(May):137–158, 2016.

[21] M. Carrara, M. R. Cacan, M. J. Leamy, M. Ruzzene, and A. Erturk. Dramatic enhancement of structure-borne wave energy harvesting using an elliptical acoustic mirror. *Applied Physics Letters*, 100(20):16–20, 2012.

[22] M. Carrara, J. A. Kulpe, S. Leadenham, M. J. Leamy, and A. Erturk. Fourier transform-based design of a patterned piezoelectric energy harvester integrated with an elastoacoustic mirror. *Applied Physics Letters*, 106(1):16–20, 2015.

[23] M Carrara, M R Cacan, J Toussaint, M J Leamy, M Ruzzene, and a Erturk. Metamaterial-inspired structures and concepts for elastoacoustic wave energy harvesting. *Smart Materials and Structures*, 22(6):065004–065012, 2013.

[24] S. Tol, F. L. Degertekin, and A. Erturk. Gradient-index phononic crystal lens-based enhancement of elastic wave energy harvesting. *Applied Physics Letters*, 109(6):1–5, 2016.

[25] K Yi, M Collet, M Ichchou, and L Li. Flexural waves focusing through shunted piezoelectric patches. *Smart Materials and Structures*, 25(7):075007, 2016.

[26] Tsung Tsong Wu, Yan Ting Chen, Jia Hong Sun, Sz Chin Steven Lin, and Tony Jun Huang. Focusing of the lowest antisymmetric Lamb wave in a gradient-index phononic crystal plate. *Applied Physics Letters*, 98(17):171911, 2011.

[27] Reddy J N. *Mechanics of Laminated Composite Plates and Shells: Theory and Analysis*. New York: CRC Press, London, second edition, 2004.

[28] Hao Zhang, Jihong Wen, Yong Xiao, Gang Wang, and Xisen Wen. Sound transmission loss of metamaterial thin plates with periodic subwavelength arrays of shunted piezoelectric patches. *Journal of Sound and Vibration*, 343:104–120, 2015.

[29] Jens Becker, Oliver Fein, Matthias Maess, and Lothar Gaul. Finite element-based analysis of shunted piezoelectric structures for vibration damping. *Computers and Structures*, 84(31-32):2340–2350, 2006.

[30] M. Collet and K.a. Cunefare. Modal Synthesis and Dynamical Condensation Methods for Accurate Piezoelectric Systems Impedance Computation. *Journal of Intelligent Material Systems and Structures*, 19(11):1251–1269, 2008.

[31] Miso Kim, John Dugundji, and Brian L Wardle. Efficiency of piezoelectric mechanical vibration energy harvesting. *Smart Materials and Structures*, 24(5):055006, 2015.

[32] Gael Matten. *Conception robuste d'actionneurs électromécaniques distribués pour le contrôle vibroacoustique de structures*. PhD thesis, Institut FEMTO-ST, 2016.

[33] Benjamin S Beck, Kenneth A Cunefare, and Manuel Collet. The power output and efficiency of a negative capacitance shunt for vibration control of a flexural system. *Smart Materials and Structures*, 22(6):065009, 2013.

[34] F. Tateo, M. Collet, M. Ouisse, and K. Cunefare. Design variables for optimizing adaptive metacomposite made of shunted piezoelectric patches distribution. *Journal of Vibration and Control*, page 1077546314545100, 2014.

[35] Gaël Matten, Manuel Collet, Scott Cogan, and Emeline Sadoulet-Reboul. Synthetic impedance for adaptive piezoelectric metacomposite. *Procedia Technology*, 15:84–89, 2014.